Optimising passivation shell thickness of single upconversion nanoparticles using a time-resolved spectrometer

Xiaoxue Xu (iD), Zhiguang Zhou, Yongtao Liu, Shihui Wen (iD), Zhiyong Guo, Laixu Gao, and Fan Wang (iD)

View Online   Export Citation   CrossMark

Optimising passivation shell thickness of single upconversion nanoparticles using a time-resolved spectrometer

View Online   Export Citation   CrossMark

Xiaoxue Xu,[1,2] (iD) Zhiguang Zhou,[1] Yongtao Liu,[1] Shihui Wen,[1] (iD) Zhiyong Guo,[1,3] Laixu Gao,[1,4] and Fan Wang[1,a)] (iD)

AFFILIATIONS

[1]Institute for Biomedical Materials and Devices (IBMD), Faculty of Science, University of Technology Sydney, NSW 2007, Australia
[2]ARC Centre of Excellence for Nanoscale BioPhotonics (CNBP), Faculty of Science, Macquarie University, NSW 2109, Australia
[3]School of Mechatronic Engineering, Southwest Petroleum University, Chengdu 610500, China
[4]School of Physical Science and Technology, Lingnan Normal University, Zhanjiang 524048, China

[a)]Author to whom correspondence should be addressed: fan.wang@uts.edu.au

ABSTRACT

Lanthanide-doped upconversion nanoparticles (UCNPs) are the most efficient multi-photon probe that can be used for deep tissue bio-imaging, fluorescence microscopy, and single molecule sensing applications. Passivating UCNPs with inert shell has been demonstrated to be an effective method to significantly enhance their brightness. However, this method also increases the overall size of the nanoparticles, which limited their cellular applications. Current reports to optimise the thickness of the shell are based on the spectrum measurement of ensembles of UCNPs, which are less quantitative. The characterisation of single UCNPs would be desirable, but is limited by the sensitivity of conventional spectrometers. We developed an optical filter-based spectrometer coupled to a laser scanning microscopy system and achieved a high degree of sensitivity−seven times more than the traditional amount. Through highly controlled syntheses of a range Yb^{3+} and Tm^{3+} doped UCNPs with different shell thickness, quantitative characterization of the emission intensity and lifetime on single UCNPs were comprehensively studied using a home-made optical system. We found that the optimal shell thickness was 6.3 nm. We further demonstrated that the system was sensitive enough to measure the time-resolved spectrum from a single UCNP, which is significantly useful for a comprehensive study of the energy transfer process of UCNPs.

INTRODUCTION

Upconversion nanoparticles (UCNPs) are typically based on NaYF$_4$ nanocrystals doped with Yb^{3+} ions as sensitisers and Tm^{3+} or Er^{3+} ions as emitters (activators). The sensitiser ions (Yb^{3+}) have relatively large absorption cross-section areas that can be used to sensitise near-infrared (e.g., 980 nm) photons. Through a network of phonon-assisted energy transfer processes, the sensitizers with high cross section areas can absorb the excitation photons efficiently and transfer to the activators. The activators typically have ladder-like multiple intermediate excited states. When one of the excited states matches that of the sensitiser ions and, most importantly, the lifetime is long enough (typically a few microseconds), the intermediate excited state can accumulate more than two sensitised photons. It can then up-convert the photons into the high energy levels of the activator to emit visible and even UV emissions.[1] Such an efficient multi-photon energy transfer process makes single UCNPs detectable under a low excitation power density of a few hundred W/cm^2. That is five orders of magnitude lower than the minimum excitation density required by conventional two-photon probes.[2,3] Hence, UCNPs are the most efficient multi-photon probe for

in vitro and *in vivo* bio-imaging,[4–6] single particle tracking,[7] deep tissue nano-thermometry sensing,[8] and near-infrared induced photothermal therapies.[9] We discovered that highly doped UCNPs are super bright in micro-structured photonic fibre or under fluorescence microscopy.[10,11] This makes them suitable for single molecule sensing. Further, we discovered that the highly doped UCNPs can easily build population inversion on one of the excited states, which helps to emit stimulated emissions under a low-power stimulated depletion laser; for example, at 808 nm, the first upconversion super-resolution nanoscopy using a low-cost low-power diode laser is enabled.[12] This suggests that UCNPs are suitable for long-term super-resolved imaging of sub-cellular structures and single bio molecules through deep tissue.

Nevertheless, developing smaller and brighter UCNPs is highly desirable for applications at cellular and sub-cellular levels. The grand challenge is their relatively large surface areas which is accessible to numerous surface quenchers. This explains why upconversion nanoparticles have significantly lower quantum efficiency than bulk crystals. In recent years, passivating UCNPs with inert shell has been found to be very useful for separating emitters away from surface quenchers, thereby significantly enhancing the brightness of UCNPs.[13,14] The passivation effect has also been found to be useful for increasing the concentrations of both sensitisers[10] and activators,[15] as well as the stability.[16] This reduces the minimum excitation power required for imaging and tuning the energy transfer process.[17–19] Conversely, the shell cannot be too thick, as thick shell results in larger sizes of UCNPs; the question of how thick it should be requires further quantitative research.[20] Ideally, it should be determined by a quantitative measurement in single nanoparticles level. However, this is currently limited by the sensitivity of the instrument available.

The characterisation of single nanoparticles will continue to advance the field of nanotechnology, quantifying each single nanoparticle and correlating their structure and growth conditions.[10,15,21,22] The simultaneous measurements of both the spectrum and the lifetime decays of a single UCNP are important to understanding its energy transfer and optical properties. However, the most of time-resolved intensity can only be measured for a broad band wavelength range.[23] Zhang *et al.* have developed a time-resolved spectroscopy system for UCNPs, yet its sensitivity cannot reach for single UCNP.[24] There have been challenges to measure the time-resolved emission spectrum for single UCNP due to its weak emissions.

Here, we developed a filter-based spectrometry optical system and applied it for single nanoparticle characterisation. Using this home-built single nanoparticle scanning confocal microscopy, the emission brightness, spectrum, and temporal domain behaviours of UCNPs with a wide range of shell thickness from 1.5 nm to 29 nm were able to be comprehensively investigated. We included both the rise time during pulsed excitation and decaying behaviours after the excitation pulses of the life time measurements for single UCNPs. We found that the optimal shell thickness of 6.3 nm resulted in the highest emission brightness for fully emitted wavelength. The shell thickness of 21.5 nm resulted in the highest brightness of 455 nm. It also resulted in the highest ratio of emission brightness—between 455 nm and 800 nm. Further, we demonstrated that the spectrometry system was sensitive enough to measure the time-resolved spectrum from a single UCNP, with the emission rate as low as 60 counts/1 ms, which is significant for the comprehensive study of energy transfer processes of UCNPs. This demonstration is also significant for UCNP multiplexing sensing that is based on both wavelength and lifetime.

RESULTS AND DISCUSSIONS

To find the optimal shell thickness, and to investigate its role in the upconversion process of UCNP, we synthesised a series of core-shell UCNPs with a wide range of shell thickness from 1.1 nm, 6.3 nm, 8.4 nm, 25.9 nm to 29.5 nm. The UCNP core is $NaYF_4$: 8% Tm^{3+}, 20% Yb^{3+} with relatively high Tm^{3+} doping
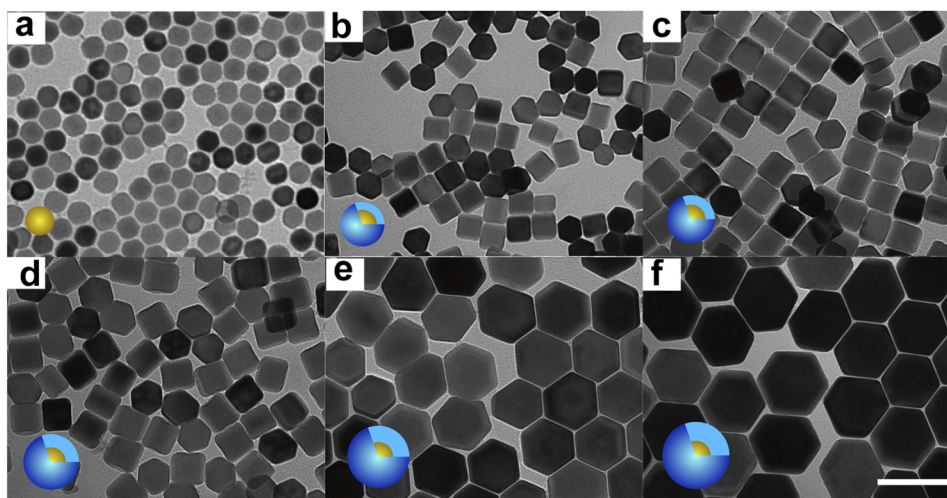
FIG. 1. TEM images of the UCNP cores of $NaYF_4$: 8% Tm^{3+}, 20% Yb^{3+} (a) and the UCNP core-shells of $NaYF_4$: 8% Tm^{3+}, 20% Yb^{3+}—$NaYF_4$ with different shell thickness of (b) 1.1 nm, (c) 6.3 nm, (d) 8.4 nm, (e) 25.9 nm, and (f) 29.5 nm. Scale bars is 100 nm.

concentration which benefits the bio-photonic applications in single nanoparticle sensing[11] and super-resolution imaging.[12] The inert shell is $NaYF_4$ without any dopants, which will only passivate the surface of UCNPs without bringing extra energy transfer. As shown in the transmission electronic microscopy (TEM) images in Fig. 1, the UCNP core is 30 nm [Fig. 1(a)] and with the shell thickness increases from 1.1 nm to 29.5 nm, the size of the core-shell UCNPs increases from 33.2 ± 1.65 nm, 43.7 ± 3.20 nm, 47.9 ± 4.52 nm, 82.9 ± 8.32 nm, and 90.0 ± 6.13 nm, as shown in Figs. 1(b)–1(f), respectively.

To do a quantitative measurement of luminescent properties of single UCNPs, we built up an optical filter-based spectrometer coupled to a laser scanning microscopy system. The microscopy system [Fig. 2(a)] was able to locate a single UCNP and capture its image. A 3D Piezo stage (Thorlabs

nanoMAX) was used to scan the testing sample. A 976.5 nm laser (Thorlabs) was focused onto the nanoparticle with a diffraction limited beam through an oil objective lens (Olympus NA 1.4). The emission was collected through a dichroic mirror, which was then directed to an optical fibre. It had a core size of 50 μm, working as a confocal pinhole with 1.01 Airy disk. The optical fibre can be connected to the designed filter-based spectrometer to measure normal spectrum and time-resolved spectrum. The optical fibre can also be connected to a single photon avalanche diode (SPAD) detector to obtain a confocal image. For spectrum measurement, the emission from the sample was input to a filter-based spectrometer [Fig. 2(b)] through the optical fibre. It was then focused onto a long pass linear variable filter (LVLWP, 310 nm-850 nm, cut-off bandwidth 3 nm, Delta) and a short pass linear variable
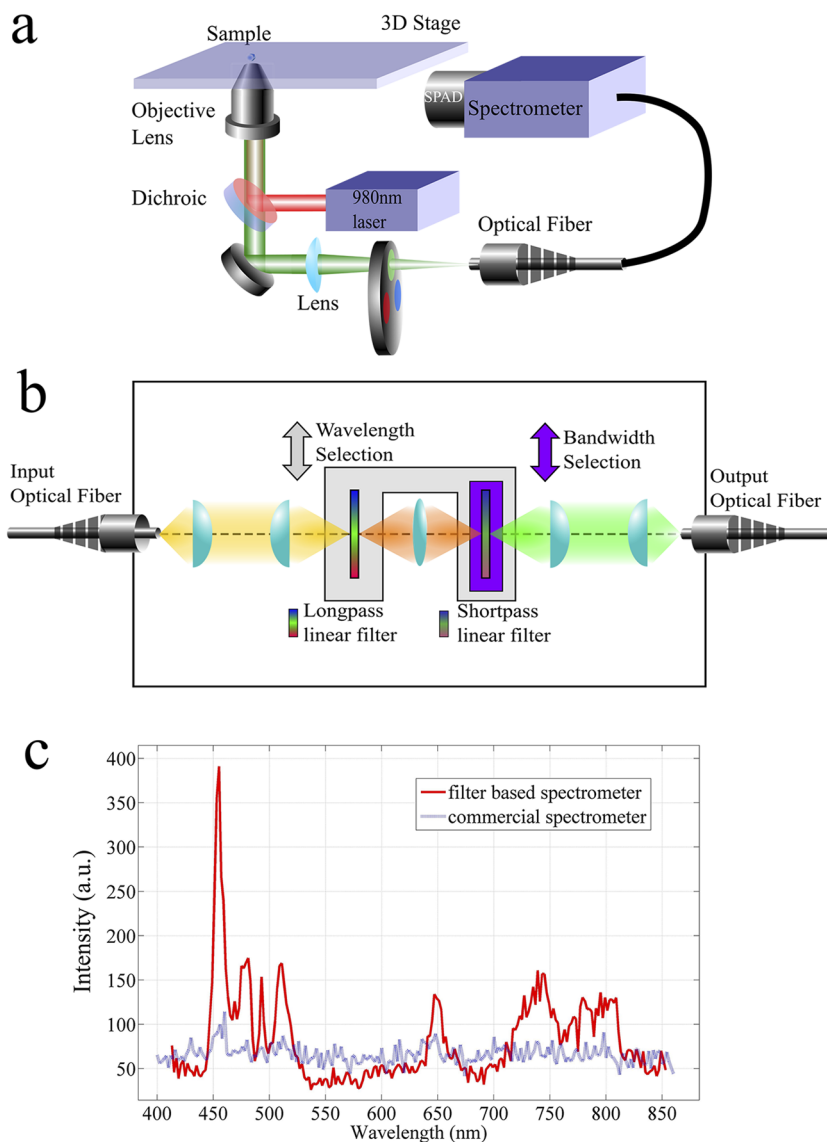
FIG. 2. (a) Laser scanning confocal microscopy system coupled with an optical filter-based spectrometer through an optical fibre. (b) The optical design of the optical filter-based spectrometer. The bandwidth of the output wavelength from the spectrometer is controlled by the relative position between the two filters that control the balances between spectrum resolution and output signal strength. The central wavelength value is selected by moving the two filters to certain positions with respect to optical axis of the system. (c) Emission spectra of a single UCNP measured by commercial spectrometer and our filter-based spectrometer with the same detector and measuring conditions.

filter (LVSWP, 320 nm-850 nm, cut-off bandwidth 3 nm, Delta Delta) to select certain output wavelengths. This was coupled to a SPAD through an optical fibre. The spectrum was measured by recording the signal from SPAD for different output wavelengths.

The emission spectrum obtained from a single UCNP using this filter-based spectrometer is shown in Fig. 2(c). Compared to the spectrum obtained from a commercial spectrometer (Horiba, Micro-HR), the emission intensity in the spectrum from our home-made spectrometer is more than seven times higher, despite the same UCNP, SPAD detector, and exposure time. This enhancement stems from the fact that a diffraction grating-based spectrometer loses part of the optical signal on other, useless diffraction orders. It suggests that the filter-based spectrometer is ideal for analysing single nanoparticles with weak emissions, such as single UCNPs with emission rates as low as 10 counts/1 ms [Fig. 2(c)]. The spectra for the suspensions of UCNPs with shells in different thickness show emission variations due to the low laser power density as shown in Fig. S1.

A quantitative comparison of emission intensity among UCNPs with different shell thicknesses is shown in Figs. 3(a) and 3(b). The quantitative measurement was conducted via the confocal imaging of single UCNPs [Fig. 3(b)]. Each Gaussian spot in the confocal image represents a nanoparticle. Its maximum pixel value indicates the brightness of the UCNP (i.e., the integrated emission intensity from all wavelengths). The emissions of UCNPs with different shell thicknesses are uniform, which is demonstrated from the mono-dispersed intensity profiles. This was used to calculate the average emission intensities and plotted as the function of shell thickness shown in Fig. 3(a). The result shows clearly that the overall emission intensity of the core-shell UCNPs was greatly enhanced with the shell coating in 1.1 nm and reached to a maximum with the 6.3 nm and 8.4 nm inert shell. With much thicker shell coating in 25.9 and 29.5 nm, the overall emission intensity slightly dropped. The enhancement of the emission intensity can be attributed to the passivation role of the inert shell preventing the surface quenching from quantum tunnelling. The maximum passivation was achieved with shell thicknesses of 6.3 nm as well as 8.4 nm owing to the ion exchange effect,[25,26] i.e., the

diffusion of sensitizer and emitter ions from the core to the inert shell. Owing to the concentration gradient from the core and the inert shell, the ion exchange would occur at the interface of the core and the shell within around 5 nm,[27-29] which results in a less effective shell thickness than the physical shell thickness and mitigated the shell passivation effect from the possibly diffused ions to the surface. Thereby, the thin shell would not passivate the surface quenching efficiently as the thicker shell; thus, the optimized surface passivation was presented with the shell in 6.3 nm and 8.4 nm for the maximum intensity. The slight decrease with even thicker shell coating could be attributed to the possible defects between the shell layers because there were two or three steps for the thick shell coatings.

To further understand the physical process of the core-shell structure, we employed spectra and time-resolved emission analysis onto single UCNPs. The emission spectra from single UCNPs with different shell thicknesses are shown in Fig. 4(a). The emission intensity values at the wavelengths of 455, 651, and 805 nm were averaged from at least 15 single UCNPs and plotted as a function of shell thickness shown in the inset of Fig. 4(a). The normalized intensity for these emissions is shown in Fig. S2. It can be seen that by increasing the shell thickness the intensity of all three emissions are enhanced and all reached to a maximum at the 6.3 nm shell and plateaued at the 8.4 nm, then there was a slight decrease with the increase in the shell thickness. This finding is consistent with the quantitative measurement conducted via the confocal imaging for the single UCNPs [Fig. 3(a)]. 6.3 nm thick inert shell is the optimized shell coating that could be attributed to the fully passivated surface on core UCNPs. The surface passivation stops the non-radiative energy transfer from sensitisers (Yb^{3+}) and emitters (Tm^{3+}) to the surface quenchers but enables more efficient energy transfer from the sensitisers (Yb^{3+}) and emitters (Tm^{3+}). Consequently, this could induce a significant increase in the rise time of low energy level (805 nm) [shown in Fig. 4(g)] due to the accumulative photons at the lower level for the inert shell passivated UCNPs. On the contrary, the photons at the lower level (805 nm) would be excited to higher levels (455 and 651 nm) inducing small increase in the rise time for higher energy levels
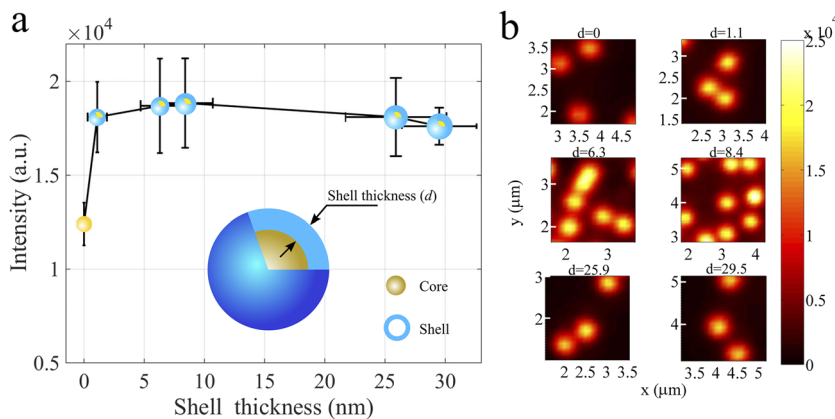

FIG. 3. Averaged luminescence intensity (a) and confocal microscopy quantitative measurement (b) of the core and core-shell nanocrystals with different shell thicknesses: 0, 1.1, 6.3, 8.4, 25.9, and 29.5 nm. The unit of colour bar is counts/50 ms.
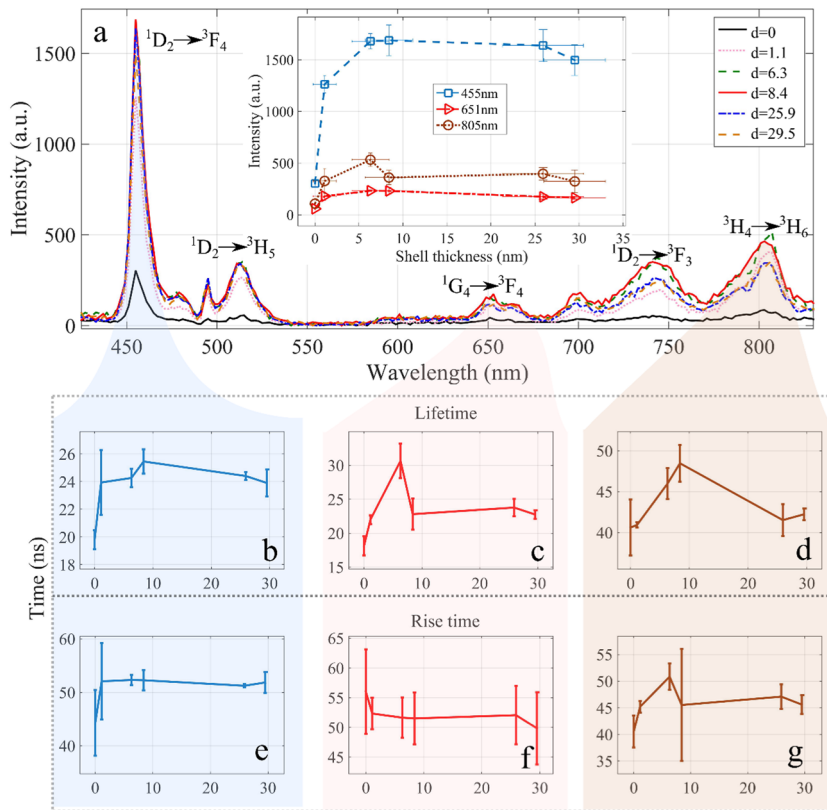
FIG. 4. (a) Spectra of single UCNPs core and core-shell nanostructures with different shell thicknesses. The inset figure is the averaged intensity values for 455 nm, 651 nm, and 805 nm emission amplitude and the energy transfer diagram. The lifetime and rise time of UCNPs emission for 455 nm [(b) and (e)], 651 nm [(c) and (f)], and 805 nm [(d) and (g)].

[shown in Figs. 4(e) and 4(f)]. This can be attributed to a lower carrier transfer rate from the sensitiser. The surface passivation also terminates the non-radiative transition path in the emitter so that the lifetimes are increased [shown in Figs. 4(b)–4(d)].

When the shell thickness increases to more than 8.4 nm, apart from the termination of the non-radiative path, two energy transfer processes start to play larger roles. As the result of the competition between the two processes, as shown in Fig. S3, the emission intensity from 455 nm ($^1D_2$ to $^3F_4$) shows less dependence on the shell thickness. Emission intensities from 651 nm ($^1G_4$ to $^3F_4$) and 805 nm ($^3H_4$ to $^3H_6$) decrease with increased shell thickness [Fig. 4(a)]. One of the processes discussed is the enhancement in upconversion efficiency. This stems from the rebalancing of carrier distribution after surface passivation. This process decreases the emission intensity from lower energy levels (651 nm and 805 nm) but increases the emission intensity from higher energy levels (455 nm). This process also decreases the rise time and lifetime on $^3H_4$ levels because more carriers move to higher energy levels [Figs. 4(d) and 4(g)]. We suggest that there is another unknown process that induces a non-radiative transition path. Its effectiveness is confirmed by the decreased lifetime on $^1D_2$ [Fig. 4(d)] and reduced intensity of 455 nm. This is despite the fact that it is balanced out by an enhanced upconversion process.

This quenching process may result from element diffusion or stress introduced internal defect during the shell growth period.
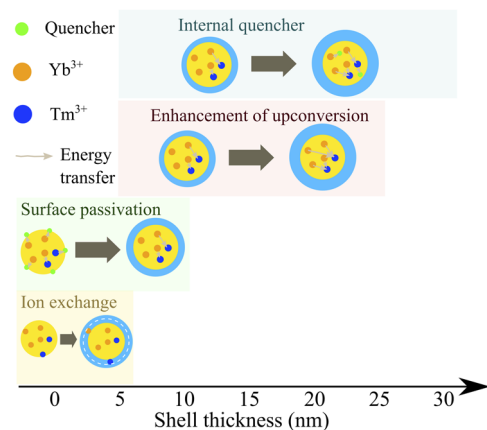
FIG. 5. The physical process for core-shell UCNPs with different shell thicknesses: ion exchange effect results in a smaller effective shell thickness (white break lines) than physical shell thickness. This difference in thickness became constant when the physical shell thickness is larger than 5 nm. Surface passivation plays a considerable role for the intensity enhancement from the thickness 0 nm to 8.4 nm. The enhancement of upconversion efficiency and internal quenchers becomes significant when the thickness is 25.9 and more.

FIG. 6. 3D (a) and 2D (c) plot of time-resolved spectrum from single 0.5 mol. % Tm^{3+} doped UCNP with 40 nm diameter. 3D (b) and 2D (d) plots of time-resolved spectrum from single 8 mol. % Tm^{3+} doped UCNP with 40 nm diameter. The horizontal lines in (c) and (d) define the laser on and off time. The vertical line marks the 800 nm position.

As the shell thickness increases to more than 20 nm, the enhancement in upconversion efficiency is mediated, which results in smaller decrease on the lower 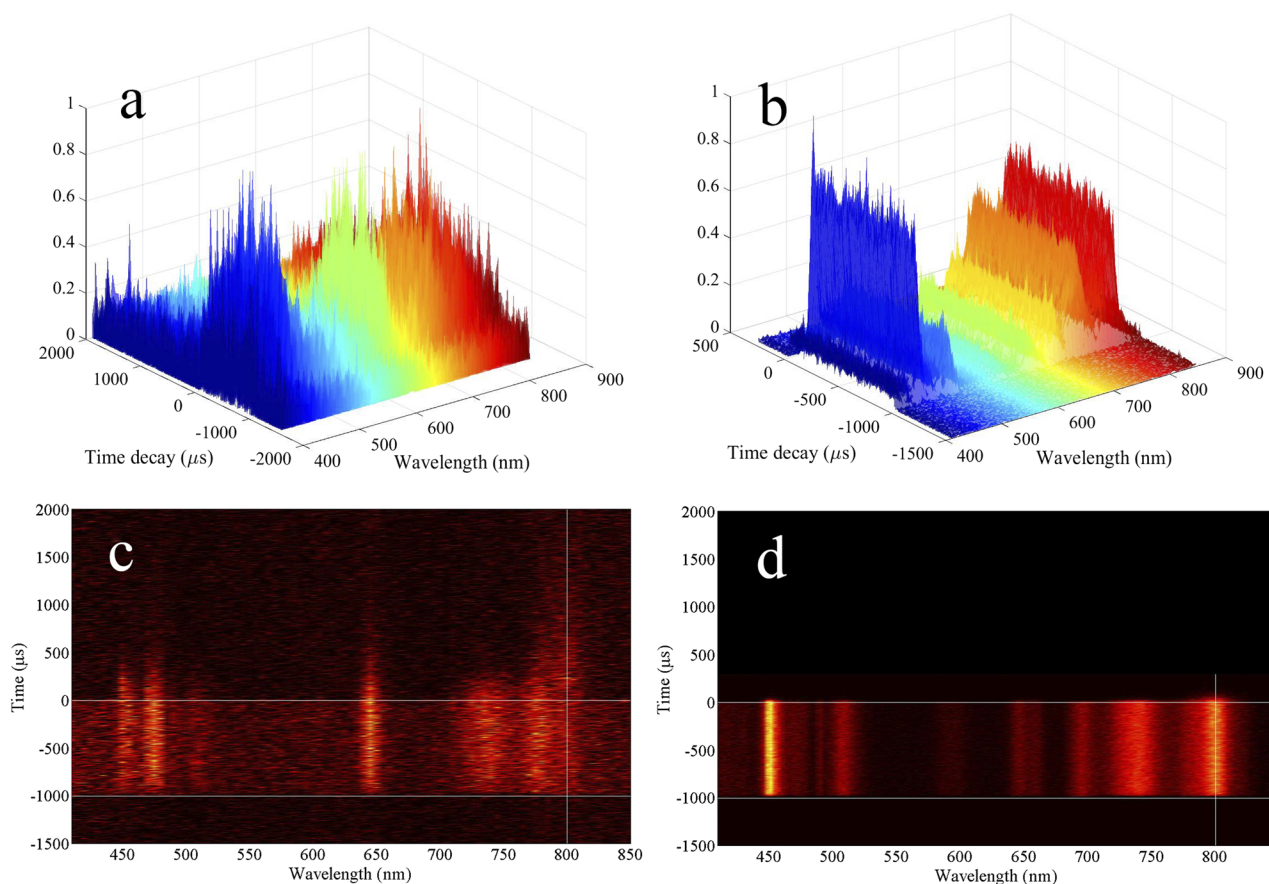energy levels (651 nm and 805 nm) shown in Figs. 4(c) and 4(d). The reduced intensity in both higher energy level and lower energy levels (455 nm, 651 nm, and 800 nm in the inset figure) indicates the non-radiative transition. In this region, the internal quencher may be increased from the interfaces between the sequent coated shells of 25.9 nm and 29.5 nm. It is worth noting that the life time of 800 nm [Fig. 4(d)] reaches its maximum when the shell thickness is 8.4 nm, in which the surface of UCNP is totally passivated. All the suggested processes discussed are shown in Fig. 5.

To further demonstrate the capability of the spectrometer, the time-resolved spectrum from a single UCNP is measured and shown in Figs. 6(a)–6(d). Figures 6(a) and 6(c) exhibit 3D and 2D plots of time-resolved spectrum on single 0.5 mol. % Tm^{3+} and 20% Yb^{3+} doped UCNP. To the best of our knowledge, this is the first demonstration of its kind. The emission intensity from the low Tm^{3+} doped UCNPs is as low as 60 photon counts/1 ms. Figures 6(b) and 6(d) show the

spectrum on a single 8 mol. % Tm^{3+} and 20% Yb^{3+} doped UCNP. For this experiment, a 980 nm laser started from −1000 μs and switched off at 0 μs, as labelled with white lines. During the laser operation period, 0.5% Tm^{3+} doped UCNP showed an extremely long rising time [Fig. 6(c)] compared with 8% Tm^{3+} doped UCNP [Fig. 6(d)]. As shown in Fig. 6(c), the emission from ^{3}H$_4$ (800 nm) was observed to reach its maximum after the laser had been switched off. This can be attributed to the energy transfer process in the sensitiser. Hence, this technology is significant for a comprehensive study of energy transfer processes, internal quantum efficiency (IQE), cross-relaxations,[30] and time-resolved multiplexing sensing.

CONCLUSION

We developed an ultra-sensitive spectrometry, and when applied, we found that the optimal shell thickness is 6.3 nm for 8% Tm^{3+} and 20% Yb^{3+} doped UCNP in terms of luminescent emission and the emission lifetime. UCNPs with 6.3 nm shell thickness showed the highest emission intensity in quantitative comparisons among UCNPs with different

shell thicknesses from 1.1 nm to 29.5 nm. The quantitative spectrum and time-resolved emissions indicated that the surface of UCNPs were gradually passivated due to increasing shell thickness until 8.4 nm. The enhancement in upconversion efficiency played an important role when the shell of the UCNP was larger than 6.3 nm and when an unknown internal quencher induced a non-radiative transition path. When the shell thickness is increased to 25.9 nm, the non-radiative quenching process from the interface of the shell coatings plays a major role in the small decrease in the intensity. Future work studying quantitative spectra for UCNPs with different Yb^{3+} and Tm^{3+} concentrations will minimise the unknown non-radiative transition and further reduce the optimised shell thickness. Furthermore, we demonstrated time-resolved spectra for 0.5% and 8% Tm^{3+} doped single UCNPs. Future work using time-resolved spectra to calculate internal quantum efficiency (IQE) for single UCNPs will advance knowledge in energy transfer processes for UCNPs.

SUPPLEMENTARY MATERIAL

See supplementary material for Detailed experimental section, size of the UCNPs and thickness of the shell calculations, colloidal suspension measurements for core and core-shell UCNPs using Fluorolog spectrophotometer, as well as the normalized emission intensity for 455 nm, 650 nm, and 805 nm from single UCNPs and core-shell UCNPs and the corresponding energy diagram for the Yb and Tm doped UCNPs.

ACKNOWLEDGMENTS

REFERENCES

[1] B. Zhou, B. Shi, D. Jin, and X. Liu, "Controlling upconversion nanocrystals for emerging applications," Nat. Nanotechnol. **10**(11), 924–936 (2015).

[2] E. M. Chan, "Combinatorial approaches for developing upconverting nanomaterials: High-throughput screening, modeling, and applications," Chem. Soc. Rev. **44**(6), 1653–1679 (2015).

[3] J. M. Watson, S. L. Marion, P. F. Rice, U. Utzinger, M. A. Brewer, P. B. Hoyer, and J. K. Barton, "Two-photon excited fluorescence imaging of endogenous contrast in a mouse model of ovarian cancer," Lasers Surg. Med. **45**(3), 155–166 (2013).

[4] S. Wu, G. Han, D. J. Milliron, S. Aloni, V. Altoe, D. V. Talapin, B. E. Cohen, and P. J. Schuck, "Non-blinking and photostable upconverted luminescence from single lanthanide-doped nanocrystals," Proc. Natl. Acad. Sci. U. S. A. **106**(27), 10917–10921 (2009).

[5] M. Nyk, R. Kumar, T. Y. Ohulchanskyy, E. J. Bergey, and P. N. Prasad, "High contrast *in vitro* and *in vivo* photoluminescence bioimaging using near infrared to near infrared up-conversion in Tm^{3+} and Yb^{3+} doped fluoride nanophosphors," Nano Lett. **8**(11), 3834–3838 (2008).

[6] C. Chen, F. Wang, S. Wen, Q. P. Su, M. C. L. Wu, Y. Liu, B. Wang, D. Li, X. Shan, M. Kianinia, I. Aharonovich, M. Toth, S. P. Jackson, P. Xi, and D. Jin, "Multi-photon near-infrared emission saturation nanoscopy using upconversion nanoparticles," Nat. Commun. **9**(1), 3290 (2018).

[7] F. Wang, S. Wen, H. He, B. Wang, Z. Zhou, O. Shimoni, and D. Jin, "Microscopic inspection and tracking of single upconversion nanoparticles in living cells," Light: Sci. Appl. **7** (2018) 18007.

[8] P. Rodríguez-Sevilla, Y. Zhang, P. Haro-González, F. Sanz-Rodríguez, F. Jaque, J. G. Solé, X. Liu, and D. Jaque, "Thermal scanning at the cellular level by an optically trapped upconverting fluorescent particle," Adv. Mater. **28**(12), 2421–2426 (2016).

[9] C. Wang, L. Cheng, and Z. Liu, "Drug delivery with upconversion nanoparticles for multi-functional targeted cancer cell imaging and therapy," Biomaterials **32**(4), 1110–1120 (2011).

[10] C. Ma, X. Xu, F. Wang, Z. Zhou, D. Liu, J. Zhao, M. Guan, C. I. Lang, and D. Jin, "Optimal sensitizer concentration in single upconversion nanocrystals," Nano Lett. **17**(5), 2858–2864 (2017).

[11] J. Zhao, D. Jin, E. P. Schartner, Y. Lu, Y. Liu, A. V. Zvyagin, L. Zhang, J. M. Dawes, P. Xi, J. A. Piper, E. M. Goldys, and T. M. Monro, "Single-nanocrystal sensitivity achieved by enhanced upconversion luminescence," Nat. Nanotechnol. **8**(10), 729–734 (2013).

[12] Y. Liu, Y. Lu, X. Yang, X. Zheng, S. Wen, F. Wang, X. Vidal, J. Zhao, D. Liu, Z. Zhou, C. Ma, J. Zhou, J. A. Piper, P. Xi, and D. Jin, "Amplified stimulated emission in upconversion nanoparticles for super-resolution nanoscopy," Nature **543**(7644), 229–233 (2017).

[13] S. Fischer, N. D. Bronstein, J. K. Swabeck, E. M. Chan, and A. P. Alivisatos, "Precise tuning of surface quenching for luminescence enhancement in core–shell lanthanide-doped nanocrystals," Nano Lett. **16**(11), 7241–7247 (2016).

[14] N. J. J. Johnson, S. He, S. Diao, E. M. Chan, H. Dai, and A. Almutairi, "Direct evidence for coupled surface and concentration quenching dynamics in lanthanide-doped nanocrystals," J. Am. Chem. Soc. **139**(8), 3275–3282 (2017).

[15] Y. Yang, Y. Zhu, J. Zhou, F. Wang, and J. Qiu, "Integrated strategy for high luminescence intensity of upconversion nanocrystals," ACS Photonics **4**(8), 1930–1936 (2017).

[16] D. Liu, X. Xu, F. Wang, J. Zhou, C. Mi, L. Zhang, Y. Lu, C. Ma, E. Goldys, J. Lin, and D. Jin, "Emission stability and reversibility of upconversion nanocrystals," J. Mater. Chem. C **4**(39), 9227–9234 (2016).

[17] R. Deng, F. Qin, R. Chen, W. Huang, M. Hong, and X. Liu, "Temporal full-colour tuning through non-steady-state upconversion," Nat. Nanotechnol. **10**, 237 (2015).

[18] X. Chen, L. Jin, W. Kong, T. Sun, W. Zhang, X. Liu, J. Fan, S. F. Yu, and F. Wang, "Confining energy migration in upconversion nanoparticles towards deep ultraviolet lasing," Nat. Commun. **7**, 10304 (2016).

[19] F. Wang, R. Deng, J. Wang, Q. Wang, Y. Han, H. Zhu, X. Chen, and X. Liu, "Tuning upconversion through energy migration in core–shell nanoparticles," Nat. Mater. **10**(12), 968–973 (2011).

[20] J. Liu, G. Chen, S. Hao, and C. Yang, "Sub-6 nm monodisperse hexagonal core/shell $NaGdF_4$ nanocrystals with enhanced upconversion photoluminescence," Nanoscale **9**(1), 91–98 (2017).

[21] C. Ma, X. Xu, F. Wang, Z. Zhou, S. Wen, D. Liu, J. Fang, C. I. Lang, and D. Jin, "Probing the interior crystal quality in the development of more efficient and smaller upconversion nanoparticles," J. Phys. Chem. Lett. **7**(16), 3252–3258 (2016).

[22] D. J. Gargas, E. M. Chan, A. D. Ostrowski, S. Aloni, M. V. P. Altoe, E. S. Barnard, B. Sanii, J. J. Urban, D. J. Milliron, B. E. Cohen, and P. J. Schuck, "Engineering bright sub-10-nm upconverting nanocrystals for single-molecule imaging," Nat. Nanotechnol. **9**(4), 300–305 (2014).

[23] Y. Lu, J. Zhao, R. Zhang, Y. Liu, D. Liu, E. M. Goldys, X. Yang, P. Xi, A. Sunna, J. Lu, Y. Shi, R. C. Leif, Y. Huo, J. Shen, J. A. Piper, J. P. Robinson, and D. Jin, "Tunable lifetime multiplexing using luminescent nanocrystals," Nat. Photonics **8**, 32 (2013).

[24] L. Zhang, A. McKay, and D. Jin, "High-throughput 3-dimensional time-resolved spectroscopy: Simultaneous characterisation of luminescence

properties in spectral and temporal domains," RSC Adv. **3**(23), 8670–8673 (2013).

[25] S. Fan, G. Gao, D. Busko, Z. Lin, S. Wang, X. Wang, S. Sun, A. Turshatov, B. S. Richards, H. Sun, and L. Hu, "Monodisperse β-NaYF$_4$:Yb^{3+},Tm^{3+} hexagonal microplates with efficient NIR-to-NIR up-conversion emission developed via ion exchange," J. Mater. Chem. C **5**(37), 9770–9777 (2017).

[26] S. Fan, G. Gao, Z. Lin, W. Li, S. Fan, S. Sun, H. Sun, and L. Hu, "Highly stable and efficient pure green up-conversion emission of rod-like β-NaGdF$_4$:Yb^{3+},Ho^{3+} submicro-crystals via ion-exchange for fluorescent labeling," J. Mater. Chem. C **6**(19), 5210–5217 (2018).

[27] D. Hudry, D. Busko, R. Popescu, D. Gerthsen, A. M. M. Abeykoon, C. Kübel, T. Bergfeldt, and B. S. Richards, "Direct evidence of significant cation intermixing in upconverting core@shell nanocrystals: Toward a new crystallochemical model," Chem. Mater. **29**(21), 9238–9246 (2017).

[28] C. Dong, A. Korinek, B. Blasiak, B. Tomanek, and F. C. J. M. van Veggel, "Cation exchange: A facile method to make NaYF$_4$:Yb,Tm-NaGdF$_4$ core–shell nanoparticles with a thin, tunable, and uniform shell," Chem. Mater. **24**(7), 1297–1305 (2012).

[29] F. Zhang, Y. Shi, X. Sun, D. Zhao, and G. D. Stucky, "Formation of hollow upconversion rare-earth fluoride nanospheres: Nanoscale Kirkendall effect during ion exchange," Chem. Mater. **21**(21), 5237–5243 (2009).

[30] B. Zhou, H. Lin, and E. Y.-B. Pun, "Tm^{3+}-doped tellurite glasses for fiber amplifiers in broadband optical communication at 1.20 μm wavelength region," Opt. Express **18**(18), 18805–18810 (2010).